

Dynamics of a Four Wheeled Wall Climbing Robot

Anokhee Chokshi^a and Jaina Mehta^b

School of Engineering and Applied Science, Ahmedabad University, Ahmedabad, Gujarat, India

Keywords: Wall Climbing Robot, Dynamic Modeling, Wheel Slip, Wheel Dynamics, Vertical Contact Forces.

Abstract: In this paper, a mathematical model of a four wheeled independently driven Wall Climbing Robot (WCR) is developed. The consideration of only the kinematic model for a WCR may reduce its performance during sudden changes in acceleration and turning. To address this issue, a dynamic model that includes the wall/wheel interactions i.e., lateral and longitudinal frictional forces, is proposed. The effect of wheel slip is considered for a more realistic dynamic model. The models that are typically developed for the vertical contact forces, an important parameter affecting the frictional forces, assume equal weight distribution on the wheels. However, to accommodate the load shift due to the variation in acceleration along with the distribution of adhesion force, lateral and longitudinal acceleration components are also taken into account. The major components of this WCR model consist of the wheel dynamics, the wall/wheel interactions, the kinematics and the dynamics. Simulations are performed to demonstrate and verify the model. The suggested model in the future can be applied in the development of control algorithms for wheeled WCRs.

1 INTRODUCTION

Wall Climbing Robots (WCR)s have been extensively studied in recent years for their potential applications in regular maintenance and inspection of urban structures that may be arduous and dangerous to work on due to their intricate construction. The use of these robots ensures safety for humans to work in hostile environments and ease in access to these structures.


Locomotion is the pivotal issue for the design of any mobile robot. In the case of a WCR, there exist different locomotion mechanisms: bio-inspired type (Chen et al., 2015), (Aksak et al., 2008), legged type (Palmer et al., 2009), (Zhan et al., 2017) and wheeled type (Faisal and Chisty, 2018), (Jun Li et al., 2009). In comparison to vehicles that travel on the ground, these robots require a potent adhesive mechanism to create a firm grip on the wall. Generally, one of the three types of adhesion mechanisms: suction cups (Shujah et al., 2019), (Sano et al., 2017), magnetic adsorption (Gong et al., 2010), (Hu et al., 2017) or thrust force (Inoue et al., 2018), (Alkalla et al., 2015) is used to solve the purpose.


In this paper, a mathematical model for a WCR which uses wheels for locomotion and thrust force for adhesion is developed. The selection of these mecha-

nisms is based on the fact that the thrust force required for adhesion, which is generated using a propeller or impeller, allows the robot to travel over surfaces with different gradients and the wheels enable the WCRs to attain higher velocities.

Several models for the dynamics of ground vehicles exist in the literature. The model developed in (Sebsadji et al., 2008) is for the case of a vehicle with two steering wheels traveling on a road with a non-zero slope angle. (Liao et al., 2019) have developed a mathematical model for a four wheel independently driven skid steer mobile robot. A model for wheel dynamics has also been presented here. (Kiencke and Nielsen, 2000) and (Wang, 2013) have introduced models for normal forces in addition to the vehicle lateral and longitudinal dynamic model for a four wheeled vehicle traveling on the ground. The theories of such models can be further extended to formulate models that establish the case of a WCR.

A considerable amount of research has been carried out for developing mathematical models for WCRs using different approaches. Most researchers ignore robot dynamics and only take kinematic models into account for the purpose of simplicity (Minzhao et al., 2015), (Gao and Kikuchi, 2004). (Panchal et al., 2014) have considered the forces acting on the WCR when it is traveling on a vertical wall. But for the vertical contact forces, equal weight dis-

^a  <https://orcid.org/0000-0003-3859-6543>

^b  <https://orcid.org/0000-0003-1972-401X>

tribution of the robot on the four wheels is assumed. (Xu and Liu, 2017) have presented a simplified model for the dynamics of a four wheeled differential drive WCR. However, the moment of inertia and the rolling friction between the wheels and the wall are ignored here. Certain other complex and complicated models, which account for obstacle avoidance have also been developed in (Xu et al., 2015) and (Ioi, 2012).

The main theme of the paper lies in the development of a dynamic model that includes the wall/wheel interactions i.e lateral and longitudinal frictional forces acting on a WCR. The major parameters affecting these frictional forces are vertical contact forces and wheel slip. In contrast to ground robots where the vertical contact forces are dependent on the weight distribution; in the case of a WCR, they depend on the adhesion force. As discussed in (Kiencke and Nielsen, 2000) and (Wang, 2013), in this paper, vertical contact forces are derived based on the load shift due to the variation in acceleration and the distribution of adhesion force on each wheel. The WCR dynamics proposed in this paper also account for the effect due to wheel slip, based on the models of rolling friction between the wheels and the ground for a mobile robot (Liao et al., 2019), (Cerkala and Jadlovska, 2014). The main contribution of this paper lies in the fact that it provides a realistic model for four wheeled WCR. The proposed model can be

used for implementing control algorithms to enhance the performance of the WCRs in the future.

The rest of the paper is organized as follows. Section 2 presents the main contribution of the proposed mathematical model. Section 3 validates the mathematical model through simulations. Section 4 draws the conclusion of the proposed mathematical model and includes future direction.

2 SYSTEM MODELING

The design of a WCR consists of two parts: locomotion and adhesion. In this paper, the WCR has four wheels for locomotion, which can be driven independently to maneuver the robot on a wall that is perpendicular to the ground. For adhesion, it is considered that the robot uses thrust force. This thrust force can be generated by the blades of a propeller or impeller, which are made to rotate such that air is thrown out from the upper side of the robot. This creates a pressure difference between the two sides of the robot and increases the friction force between the wheels of the robot and the wall. Figure 1 represents the forces acting on a WCR when it is placed on the wall.

In this paper, it is assumed that all the wheels are in contact with the wall at all times. This implies that there is no roll or pitch motion of the robot. It is also

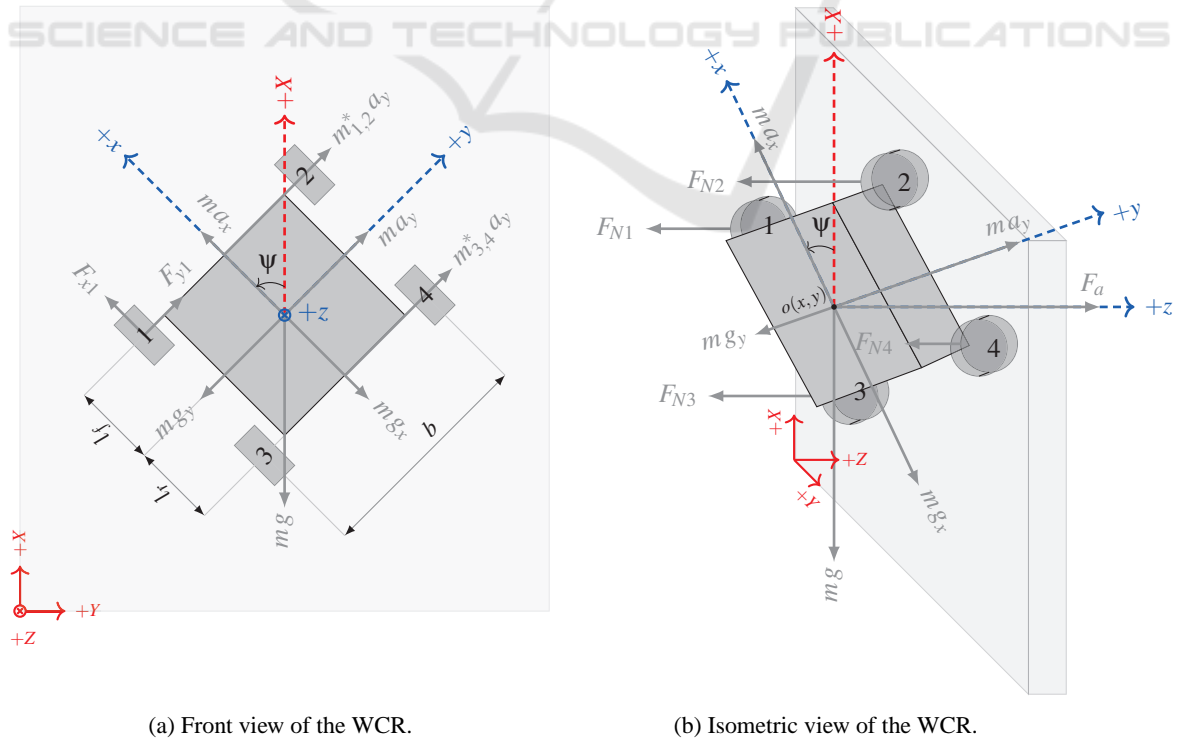


Figure 1: Representation of the forces acting on the WCR when it is at an arbitrary angle ψ .

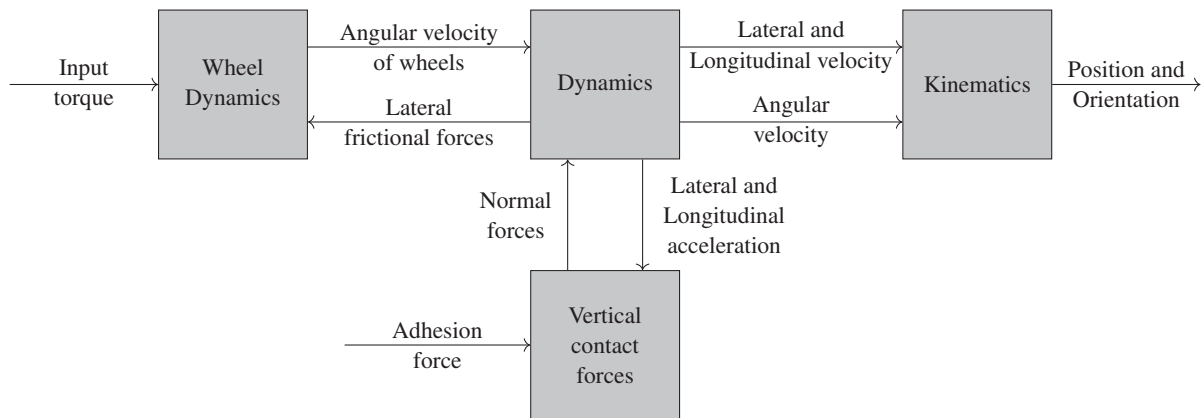


Figure 2: Mathematical model of the WCR.

assumed that the centre of mass is the same as the geometrical centre of the robot. A thrust force F_a , which creates enough adhesion for the robot to stick to the wall, acts perpendicular to the wall.

As per Figure 1, let XYZ be the global co-ordinate system and xyz be the co-ordinate system attached to the robot. (X, Y) and ψ are the position and orientation of the robot with respect to the global co-ordinate system. l_r and l_f represent the distance between the centre of mass and the centres of the rear wheel and the front wheel respectively, b is the distance between the left and right wheels and H is the distance between the centre of mass and the wall. m is the mass of the robot. The gravitational acceleration acts in the $-X$ direction and has two components in x and y direction in the local co-ordinate frame that is attached to the robot, denoted by $g_x = g \cos \psi$ and $g_y = g \sin \psi$.

The mathematical model that is proposed in this paper is illustrated by the block diagram in Figure 2. It consists of four parts - the dynamics of the wheel, which give a relation between the input torque and angular velocity of each wheel while taking the damping effect into account; the vertical contact forces on each wheel; the WCR dynamics, which include the effect of wheel slip; and the kinematics of the WCR, which give the position and orientation of the robot w.r.t. the global co-ordinates. The model of each sub-part is discussed in detail in the subsequent sub-sections.

2.1 Vertical Contact Forces

When the mobile robot travels on the ground, the total vertical force is caused by the force due to the earth's gravitational acceleration. Whereas, when the robot is traveling on a wall, which is perpendicular to the ground, the total vertical force is caused due to the adhesion force. Apart from adhesion force, other factors like the longitudinal and lateral acceleration of

the robot chassis and the geometry of the robot are considered in determining the normal force on each wheel as discussed in (Kiencke and Nielsen, 2000), (Wang, 2013). However, certain other factors like the wall surface geometry and air resistance are not considered and some reasonable simplifications are made for reducing the complexity.

The contact forces alter as the vehicle acceleration changes. Due to inertia, the acceleration of the chassis (a_{xc} , a_{yc}) is in the opposite direction of the longitudinal and lateral accelerations (a_x , a_y) i.e. when the robot accelerates in the forward direction, the chassis accelerates in the backward direction because the wheel load shifts to the rear axle. Hence, $a_{xc} = -a_x$ and $a_{yc} = -a_y$.

Since it is assumed that there is no pitch, the force due to acceleration in the $+x$ -direction causes a torque which reduces the load on the front axle and increases the load on the rear axle. Here, axle is an imaginary line that connects the centres of the front wheels or rear wheels. As seen in Figure 1 (b), the normal force acting on the front wheels (F_{N1}, F_{N2}) is given by calculating the total moment on the rear axle.

$$(F_{N1} + F_{N2})(l_r + l_f) = -ma_{xc}H - mg_xH + F_a l_r \quad (1)$$

The front and the rear axle are assumed to be decoupled. As seen in Figure 1, $m_{1,2}^*$ and $m_{3,4}^*$ denote the virtual mass present at the front and rear axle respectively. They can be expressed as $m_{1,2}^* = (F_{N1} + F_{N2})/a_z$ and $m_{3,4}^* = (F_{N3} + F_{N4})/a_z$, where a_z is the acceleration in the direction perpendicular to the wall. Based on Equation (1), the virtual mass at the front axle can be rewritten as:

$$m_{1,2}^* = -\frac{m^2 a_{xc} H}{F_a (l_r + l_f)} - \frac{m^2 g \cos \psi H}{F_a (l_r + l_f)} + \frac{m(l_r)}{(l_r + l_f)} \quad (2)$$

Since it is also assumed that there is no roll, as shown in Figure 1, considering the torque balance at

the front right wheel, the normal force acting on the front left wheel is calculated as:

$$F_{N1}(b) = m_{1,2}^* a_z (b/2) + m_{1,2}^* a_{yc} H + m_{1,2}^* g_y H \quad (3)$$

When the longitudinal and lateral coupling is not taken into account, the equations of the normal forces acting on each wheel can be expressed as:

$$\begin{aligned} F_{N1} &= -\frac{m(a_{xc} + g \cos \psi)H}{2(l_r + l_f)} + \frac{F_a(l_r)}{2(l_r + l_f)} \\ &\quad + \frac{m(l_r)(a_{yc} + g \sin \psi)H}{(b)(l_r + l_f)} \\ F_{N2} &= -\frac{m(a_{xc} + g \cos \psi)H}{2(l_r + l_f)} + \frac{F_a(l_r)}{2(l_r + l_f)} \\ &\quad - \frac{m(l_r)(a_{yc} + g \sin \psi)H}{(b)(l_r + l_f)} \\ F_{N3} &= \frac{m(a_{xc} + g \cos \psi)H}{2(l_r + l_f)} + \frac{F_a(l_f)}{2(l_r + l_f)} \\ &\quad + \frac{m(l_f)(a_{yc} + g \sin \psi)H}{(b)(l_r + l_f)} \\ F_{N4} &= \frac{m(a_{xc} + g \cos \psi)H}{2(l_r + l_f)} + \frac{F_a(l_f)}{2(l_r + l_f)} \\ &\quad - \frac{m(l_f)(a_{yc} + g \sin \psi)H}{(b)(l_r + l_f)} \end{aligned} \quad (4)$$

The above equations consider the effect of adhesion force; and the longitudinal and lateral accelerations on the vertical contact force acting on each wheel.

2.2 Kinematic Model of the WCR

Based on the orientation of the co-ordinate systems as shown in Figure 1, the kinematic model of the WCR is expressed as:

$$\begin{aligned} \dot{X} &= v_x \cos(\psi) + v_y \sin(\psi) \\ \dot{Y} &= -v_x \sin(\psi) + v_y \cos(\psi) \\ \dot{\psi} &= \omega \end{aligned} \quad (5)$$

(v_x, v_y) denote the velocity of the robot in the x and y directions respectively and ω is the angular velocity of the robot.

2.3 Dynamic Model of the WCR

The dynamic model of the WCR considering slip compensation is expressed as:

$$\begin{aligned} m \dot{v}_x &= \sum_{i=1}^4 F_{xi} + m v_y \omega - m g_x \\ m \dot{v}_y &= \sum_{i=1}^4 F_{yi} - m v_x \omega - m g_y \\ \ddot{\psi} &= \frac{1}{I_z} \sum_{i=1}^4 M_{zi} \end{aligned} \quad (6)$$

F_{xi} and F_{yi} are the longitudinal and lateral frictional forces. The moment around z-axis is given by M_{zi} and the moment of inertia around z-axis is I_z .

Generally, in the case of ground robots, the friction forces acting against the mobile robot are ignored with the assumption of pure rolling. However, it becomes necessary to include them in the dynamic model of the WCR since there will be no adhesion in their absence. A simplified model for friction forces due to ground and wheel interactions based on (Liao et al., 2019) is used.

$$F_{xi} = F_{Ni} \mu_r S_f(s_i) \frac{s_{xi}}{s_i}$$

$$F_{yi} = F_{Ni} \mu_s S_f(s_i) \frac{s_{yi}}{s_i}$$

$$\begin{aligned} \sum_{i=1}^4 M_{zi} &= l_f(F_{y1} + F_{y2}) + \frac{b}{2}(-F_{x1} + F_{x2} \\ &\quad - F_{x3} + F_{x4}) - l_r(F_{y3} + F_{y4}) \end{aligned} \quad (7)$$

F_{Ni} are the normal forces which are calculated in Section 2.1. ; μ_r and μ_s are the rolling and sliding co-efficients of friction; s_{xi} and s_{yi} represent the longitudinal and lateral slip for each wheel and can be calculated as:

$$\begin{aligned} s_{x1} &= r\omega_{r1} - v_x + (b/2)\omega, s_{y1} = v_y + l_f\omega \\ s_{x2} &= r\omega_{r2} - v_x - (b/2)\omega, s_{y2} = v_y + l_f\omega \\ s_{x3} &= r\omega_{r3} - v_x + (b/2)\omega, s_{y3} = v_y - l_r\omega \\ s_{x4} &= r\omega_{r4} - v_x - (b/2)\omega, s_{y4} = v_y - l_r\omega \end{aligned} \quad (8)$$

ω_{ri} is the angular velocity of each wheel. This is obtained using the input torque on each wheel described in the following sub-section. From Equation (8), $s_i = \sqrt{s_{xi}^2 + s_{yi}^2}$ and the dynamic feature of the friction force can be approximated as: $S_f(s_i) = \frac{2}{\pi} \text{atan}(90s_i)$.

2.4 Wheel Dynamics

The rotational dynamics of each wheel are derived from Figure 3.

$$J_{ri} \dot{\omega}_{ri} + c_{ri} \omega_{ri} = u_{ri} - r F_{xi} \quad (9)$$

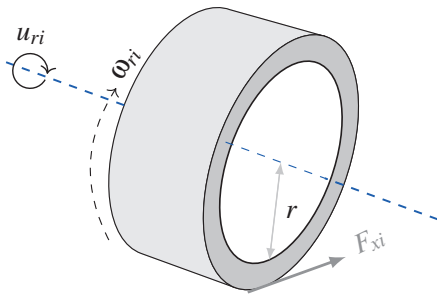


Figure 3: Wheel rotational motion.

J_{ri} represents the moment of inertia, c_{ri} is the damping co-efficient, ω_{ri} is the angular velocity, u_{ri} denotes the input torque and r is the radius of the wheel.

3 SIMULATION RESULTS

The realistic dynamic model that includes wall and wheel interactions and wheel slip for the WCR is simulated in the Simulink environment. The response of the proposed model is generated with different robot orientations and by providing different input torques to the robot wheels. The solution of the model equations is obtained by ode45 solver, with the error tolerance set to 10^{-4} and the simulation time set to 20 s. The lateral velocity and its derivatives are bounded based on the robot geometry and physical constraints.

For the purpose of the simulation, it is considered that $b = 610 \times 10^{-3} m$, $l_f = 175.01 \times 10^{-3} m$, $l_r = 175.01 \times 10^{-3} m$, $H = 33.38 \times 10^{-3} m$, $r = 35 \times 10^{-3} m$, $c_{ri} = 0.1 N/m$, $J_{oi} = 3.68 \times 10^{-5} kg m^2$, $\mu_r = 0.5$, $\mu_s = 0.9$, $m = 1.75 kg$, $I_z = 11.74 \times 10^{-2} kg m^2$ and $F_a = 51.5 N$.

As illustrated in Figure 4, for Case 1, when the WCR is initially at $\psi = 0$, a constant and identical input torque is given to all the four wheels for the first time interval. This results in the upward movement of the WCR i.e. movement in the +X direction. Due to the consideration of lateral frictional forces, minor changes in the orientation of the robot ψ and movement in the Y-axis are observed. In the second time interval, the input torque of the same magnitude but opposite in direction is given to all four wheels. This produces results similar to the first interval. However, the movement of the robot is in reverse direction i.e. in the -X direction. It is important to note that the same magnitude of torque in the reverse direction in this case produces a greater amount of change in the position of the robot. This is caused due to the gravitational acceleration acting in the -X direction. No torque is given to the wheels in the third interval. As

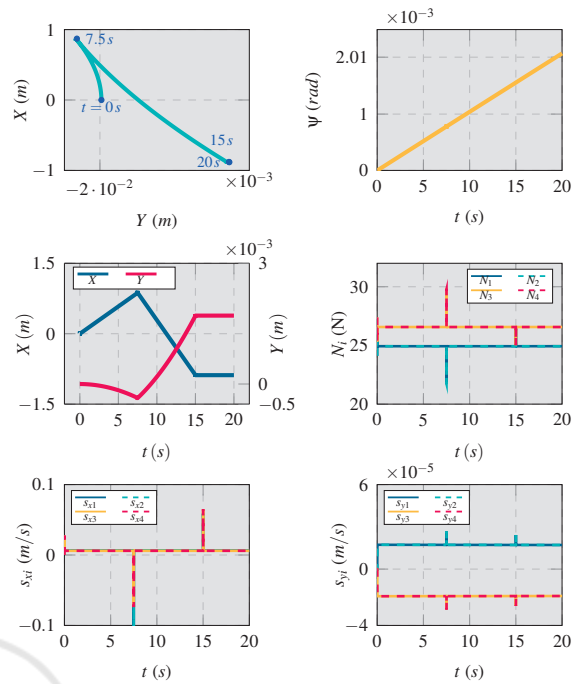


Figure 4: (Case 1) : $(X_0, Y_0) = (0, 0)$; $\psi_0 = 0$; $u_{ri} = 0.5 Nm$ ($0 \leq t \leq 7.5$); $u_{ri} = -0.5 Nm$ ($7.5 < t \leq 15$) and $u_{ri} = 0 Nm$ ($15 < t \leq 20$).

the robot is in motion, it takes a finite time for it to preserve its final position in X and Y directions.

It can be observed from the wheel slip graphs in Figure 4 that when a constant and identical input torque is given to all four wheels, the wheel slip is close to zero. At $t = 7.5 s$ and $t = 15 s$, i.e. at the points when the torque value changes, there is a sudden change in wheel slip.

The longitudinal and lateral accelerations are zero when the input torque is constant. It can be observed from Figure 4 that the normal forces remain constant for each time interval as the only other factors affecting them are the gravitational acceleration and adhesion force, which are constant. A sudden change is seen only at the points when the input torque is changed.

Figure 5 illustrates the results of Case 2, where the input torque remains the same as Case 1, but the initial orientation of the robot is changed to $\psi = \pi/2$. This means that the robot would replicate the movement of the robot as in Case 1, but in the Y-axis instead. However, due to the absence of gravitational acceleration in the direction of movement of the robot, when the robot is at an angle $\psi = \pi/2$, the same magnitude of torque in the reverse direction in the second time interval would result in the same change in position as seen in the first time interval. In this case, the effect of lateral frictional forces is seen in the X-direction.

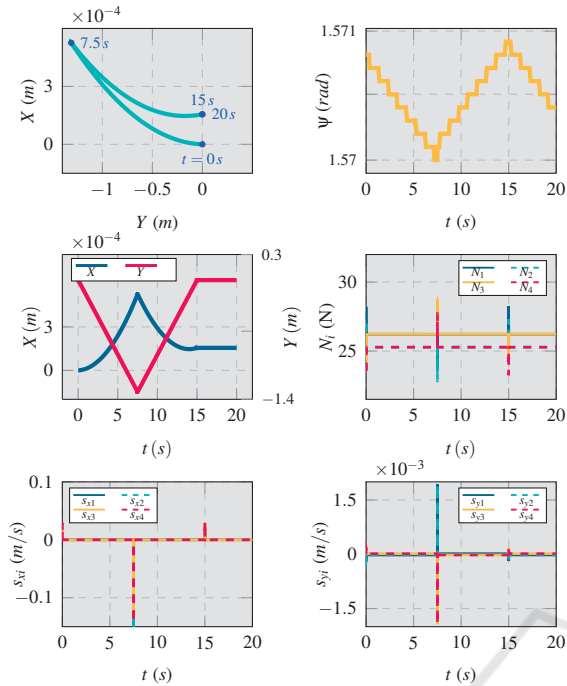


Figure 5: (Case 2) : $(X_0, Y_0) = (0, 0)$; $\psi_0 = \pi/2$; $u_{ri} = 0.5 \text{ Nm}$ ($0 \leq t \leq 7.5$); $u_{ri} = -0.5 \text{ Nm}$ ($7.5 < t \leq 15$) and $u_{ri} = 0 \text{ Nm}$ ($15 < t \leq 20$).

Observations similar to Case 1 can be made for the wheel slip and the normal forces acting on each wheel in Case 2.

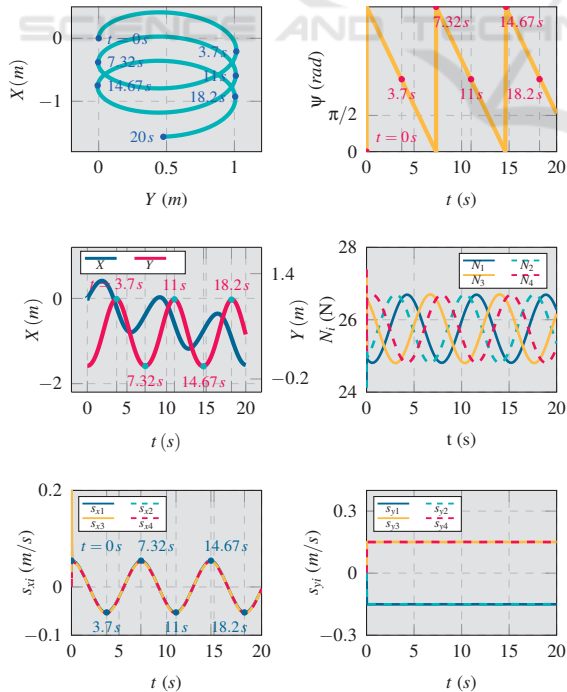


Figure 6: (Case 3) : $(X_0, Y_0) = (0, 0)$; $\psi_0 = 0$; $u_{r(1,3)} = 2 \text{ Nm}$ and $u_{r(2,4)} = 0.5 \text{ Nm}$ ($0 \leq t \leq 20$).

As illustrated in Figure 6, in Case 3, wheels on the left are given higher torque than the wheels on the right. This type of differential input torque results in a turn-like movement of the robot in the clockwise direction. Therefore, change in both X and Y directions is seen here.

In this case, a continuous change in the longitudinal wheel slip is observed. The wheel slip takes both positive and negative values. Based on Equation (8), the positive value of the s_{xi} indicates slipping and the negative value indicates the skidding of the wheel. The change in the longitudinal wheel slip in Case 3 is due to differential input torque, which leads to a continuous change in the orientation. When the orientation of the robot is $\pi/2$ or $3\pi/2$, the slip value is near to zero.

The maximum skid is observed when $\psi = \pi$ and maximum slip is observed when $\psi = 2\pi$. It is important to note that if the difference between the input torques of the left and right wheels is increased, it will increase the magnitude of wheel slip.

Since the robot is turning, the longitudinal and lateral acceleration of the robot changes constantly. This leads to continuously changing normal forces on each wheel.

4 CONCLUSION

This paper introduces a more realistic dynamic model of a four wheeled WCR by considering wheel slip and vertical contact forces on each wheel. The simulations are based on reasonable assumptions for the physical constraints of the WCR when it is traveling on the wall. The analysis of these simulations for different conditions of input torque suggests that the model is valid. The simulations also reveal that input wheel torque and the orientation are factors that affect the wheel slip and vertical contact forces of the WCR.

The current model only allows the yaw motion of the robot with the consideration that all the wheels are in contact with the wall at all times. Therefore, as future work, adding the consideration of pitch and roll will allow the model to be suitable even for the wall surfaces that are irregular or not flat. Moreover, the implementation of control algorithms in the proposed model will enable the derivation of optimal values for the parameters like adhesion force and input torques for the wheels. Subsequently, a physical model can be constructed and the proposed mathematical model can be verified experimentally.

ACKNOWLEDGEMENTS

The authors would like to express their gratitude to Dr. Harshal Oza (Associate Professor, Pandit Deendayal Energy University) for his insights and expertise which supported the research.

REFERENCES

- Aksak, B., Murphy, M. P., and Sitti, M. (2008). Gecko inspired micro-fibrillar adhesives for wall climbing robots on micro/nanoscale rough surfaces. In *2008 IEEE International Conference on Robotics and Automation*, pages 3058–3063.
- Alkalla, M. G., Fanni, M. A., and Mohamed, A.-F. (2015). Versatile climbing robot for vessels inspection. In *2015 International Conference on Control, Automation and Robotics*, pages 18–23.
- Cerkala, J. and Jadlovská, A. (2014). Mobile robot dynamics with friction in simulink. In *22th Annual Conference Proceedings of the International Scientific Conference - Technical Computing Bratislava 2014*.
- Chen, J., Li, G., Zhang, J., and Yu, J. (2015). Caterpillar-like climbing method incorporating a dual-mode optimal controller. *IEEE Transactions on Automation Science and Engineering*, 12(4):1492–1503.
- Faisal, R. H. and Chisty, N. A. (2018). Design and implementation of a wall climbing robot. *International Journal of Computer Applications*, 179(13):1–5.
- Gao, X. and Kikuchi, K. (2004). Study on a kind of wall cleaning robot. In *2004 IEEE International Conference on Robotics and Biomimetics*, pages 391–394.
- Gong, Y., Wang, Z., Wang, X., and Xu, J. (2010). Analysis on turning stress states of magnetic sucking mechanism unit of a large load wall climbing robot. In *2010 International Conference on Measuring Technology and Mechatronics Automation*, volume 1, pages 570–573.
- Hu, S., Peng, R., He, K., Li, J., Cai, J., and Zhou, W. (2017). Structural design and magnetic force analysis of a new crawler-type permanent magnetic adsorption wall — climbing. In *2017 IEEE International Conference on Information and Automation (ICIA)*, pages 598–603.
- Inoue, F., Honjo, A., Makino, T., and Kwon, S. (2018). Inspection robot system using duct fan and deterioration estimation of building wall that can be applied even in disaster. In *2018 18th International Conference on Control, Automation and Systems (ICCAS)*, pages 331–334.
- Ioi, K. (2012). Design of wall-climber with coaxial propeller’s thruster. In *The 43th International Symposium on Robotics At: Taipei*, pages 168–172.
- Jun Li, Xueshan Gao, Ningjun Fan, Kejie Li, and Zhihong Jiang (2009). Bit climber: A centrifugal impeller-based wall climbing robot. In *2009 International Conference on Mechatronics and Automation*, pages 4605–4609.
- Kiencke, U. and Nielsen, L. (2000). *Automotive Control Systems: For Engine, Driveline and Vehicle*. Springer-Verlag, Berlin, Heidelberg, 1st edition.
- Liao, J., Chen, Z., and Yao, B. (2019). Model-based coordinated control of four-wheel independently driven skid steer mobile robot with wheel–ground interaction and wheel dynamics. *IEEE Transactions on Industrial Informatics*, 15(3):1742–1752.
- Minzhao, X., Jichen, L., and Xiaoyi, L. (2015). The innovation design of the magnetic adsorption climbing-wall flaw detection robot. In *The 27th Chinese Control and Decision Conference (2015 CCDC)*, pages 4923–4926.
- Palmer, L. R., Diller, E. D., and Quinn, R. D. (2009). Design of a wall-climbing hexapod for advanced maneuvers. In *2009 IEEE/RSJ International Conference on Intelligent Robots and Systems*, pages 625–630.
- Panchal, K., Vyas, C., and Patel, D. (2014). Developing the prototype of wall climbing robot. In *International Journal of Advance Engineering and Research Development [IJAERD]*, Issue 3, volume 1.
- Sano, S., Ohara, K., Ashizawa, S., Ichikawa, A., Suzuki, S., Omichi, T., and Fukuda, T. (2017). Development of wall climbing robot using passive joint and vacuum pad on rough surface. In *2017 International Symposium on Micro-NanoMechatronics and Human Science (MHS)*, pages 1–3.
- Sebsadji, Y., Glaser, S., Mammari, S., and Dakhilallah, J. (2008). Road slope and vehicle dynamics estimation. In *2008 American Control Conference*, pages 4603–4608.
- Shujah, A., Habib, H., Shaikh, S., Ishfaq, A. R., Tahir, H., and Iqbal, J. (2019). Design and implementation of semi-autonomous wall climbing robot using vacuum suction adhesion. In *2019 IEEE 17th World Symposium on Applied Machine Intelligence and Informatics (SAMII)*, pages 275–280.
- Wang, B. (2013). *State observer for diagnosis of dynamic behavior of vehicle in its environment*. Theses, Université de Technologie de Compiègne.
- Xu, F., Shen, J., and Jiang, G. (2015). Kinematic and dynamic analysis of a cable-climbing robot. *International Journal of Advanced Robotic Systems*, 12:1.
- Xu, Y. and Liu, R. (2017). Concise method to the dynamic modeling of climbing robot. *Advances in Mechanical Engineering*, 9:168781401769167.
- Zhan, Q., Yang, L., Zhang, Y., Ma, Y., and Rahmani, A. (2017). Research on torque optimization of biped wall climbing robot based on genetic algorithm. In *2017 International Conference on Computer Technology, Electronics and Communication (ICCTEC)*, pages 1030–1035.